

Numerical Method for Hydrodynamic Transport of Inhomogeneous Polymer Melts

David M. Hall^{a,c} Turab Lookman^c Glenn H. Fredrickson^b
Sanjoy Banerjee^b

^a *Department of Physics, University of California, Santa Barbara, CA 80310*

^b *Department of Chemical Engineering, University of California, Santa Barbara,
CA 80310*

^c *Theoretical Division, Los Alamos National Laboratory, Los Alamos, NM 87545*

Abstract

We describe in detail a mesoscale method for simulating hydrodynamic transport of inhomogeneous polymer melts in arbitrary channel geometries. The method employs non-equilibrium self consistent field theory to describe block copolymer self assembly, viscoelastic multiple-fluid hydrodynamics to model material transport, and rigid wall fields to represent channel boundaries and machine components. We present a fast, pseudo-spectral solution for these equations and validate it by performing convergence studies on several challenging problems in both two and three dimensions, including the flow of a viscous fluid at low Reynolds number past a fixed sphere and phase separation of diblock copolymer melts that have been quenched into the intermediate segregation regime.

1 Introduction

In industrial processing flows such as melt injection, blow moulding, spin coating, and fiber drawing, incompatible polymeric components are driven by thermodynamic forces to phase separate while simultaneously being mixed and aligned by the flow. In many cases, the quality of the final product produced by these processes depends in detail on non-equilibrium, defect filled states which become kinetically trapped when the melt is quenched to room temperature. For block copolymer melts it is often desirable to employ shearing flows which remove defects and assist self assembly in order to induce long range order. On the other hand, macro-phase separation is usually undesirable for blends of incompatible homopolymers, and processing conditions which keep

the components well mixed are preferred. Furthermore, preferential wetting of the boundary surfaces and the presence of surfactants or solid contaminants can strongly modify the dynamics, complicating the situation.

Although much attention has been devoted to the development of methods for predicting equilibrium properties of block copolymer melts [1–3], simulation of non-equilibrium states is less well understood. While molecular dynamics simulations are ideal for predicting polymer dynamics at atomistic scales, mesoscale methods are more appropriate for larger systems. Dynamic self consistent field theory (DSCFT) represents one of the most successful techniques [4–9] designed to examine non-equilibrium states at mesoscopic scales, and the scheme we have developed falls into this category as well. Unlike previous DSCFT techniques, however, the method we have constructed focuses on systems in which hydrodynamic transport plays a central role, and we refer to it as hydrodynamic self consistent field theory (HSCFT) to underscore this emphasis. The method combines non-equilibrium self consistent field theory with multiple-fluid hydrodynamics and a set of constitutive equations that track viscoelastic stresses. In addition, it employs rigid wall fields to model arbitrary channel geometries and moving machine parts, with preferential wetting by one or more components. The role of each component in the model and their interactions is outlined in Fig. 1. The addition of rigid walls allows us to generate a range of hydrodynamic environments, and it provides a means of measuring force-feedback on the machine elements, enabling rheological measurements.

In section 2 of this paper, we present a non-equilibrium mesoscale thermodynamic model for a melt of several linear copolymers in the presence of rigid walls. In section 3, we apply Rayleigh’s variational principle to derive a multiple-fluid hydrodynamic model for a mixture of viscoelastic fluids. In section 4 we convert the equations to dimensionless form, and in section 5 we present a numerical solution that makes extensive use of pseudospectral methods. We validate the scheme in sections 6 and 7 by performing convergence studies on several challenging problems including the flow of a homopolymer band past a fixed spherical obstacle at low Reynolds number, and the phase separation of symmetric and asymmetric quenched diblock copolymer melts. Finally, we summarize our work.

2 Thermodynamics of Copolymer Blends with Rigid Walls

In this section, we construct a non-equilibrium, field theoretic model that describes a melt of multiple linear copolymers in the presence of rigid channel walls. Following the procedure outlined in [10], we construct a mesoscale model of the essential physics, convert it to field theoretic form, and then

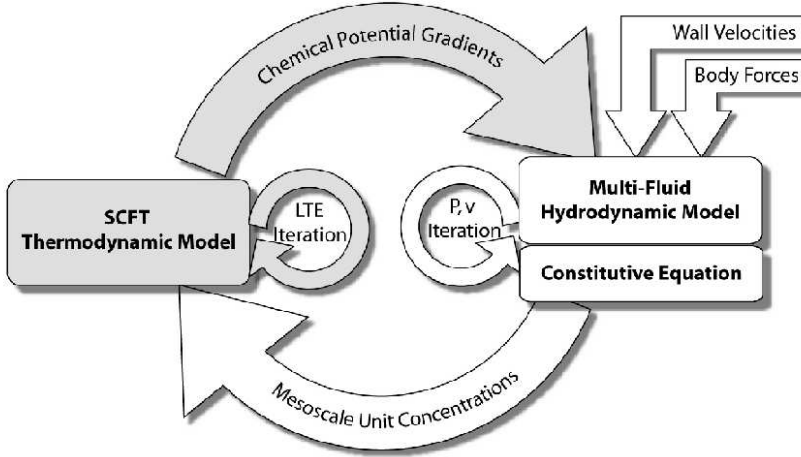


Fig. 1. Overview of HSCFT scheme. The SCFT thermodynamic model iterates to find chemical potentials that are consistent with local thermodynamic equilibrium (LTE) conditions. The imbalanced chemical potential gradients, moving wall fields, and applied body forces induce hydrodynamic flow. The viscoelastic multi-fluid model iterates to find pressure and velocity fields that simultaneously satisfy the zero Reynolds number momentum balance condition and incompressibility. These velocity fields are then used to transport the volume fraction fields.

apply a mean field approximation to obtain the chemical potential gradients that drive microphase separation.

2.1 Mesoscale Model Construction

The system can be visualized as a densely packed array of mesoscale units, each of which occupies an equal volume in the melt. A copolymer is represented as a long flexible chain of connected mesoscale units (monomers), and the channel walls are similarly represented as large collections of rigidly connected units. In the most general case, the melt consists of C distinguishable copolymer species, each of which has polymerization index N_α and entanglement length $N_{e\alpha}$. There are n_α^ϕ copies of each copolymer species. Each copolymer is constructed from M_α^ϕ chemically distinct monomers, and the monomer occupation function $\gamma_{\alpha i}(s)$ parameterizes their distribution along the chain, with $s \in [0..1]$. There are also M^ψ chemically distinct mesoscale wall units. The volume occupied by each mesoscale unit in the melt is therefore $v_0 = V / (\bar{N} \sum_\alpha n_\alpha^\phi + \sum_j n_j^\psi)$ where the average polymerization index is $\bar{N} = \sum_\alpha n_\alpha^\phi N_\alpha / \sum_\beta n_\beta^\phi$.

The essential forces in the system consist of the interactions due to covalent bonds between connected mesoscale units, a hard core steric repulsion that prevents overlap, Van der Waals attractions between each unit, and an entropic tendency for an extended polymer to contract. The covalent bonds

between monomers are modeled implicitly by the connectivity of the parameterized space curves $\mathbf{R}_{\alpha j}^\phi(s)$ where the first index indicates the copolymer species $\alpha \in \{1\dots C\}$ and the second index runs over all instances of that species $j \in \{1\dots n_\alpha^\phi\}$. Similarly, the covalent bonds between mesoscale wall units are modeled by treating each collection as a single rigidly rotating and translating object. The hard core repulsion is also treated implicitly by enforcing the incompressibility of the melt, $\nabla \cdot \mathbf{v} = 0$.

An unperturbed polymer in the melt resembles a random walk, and stretching it results in an entropically disfavored state. If the copolymer is not stretched too far, this entropic penalty can be approximated by an equivalent harmonic potential energy (called the Gaussian thread approximation.)

$$H_0/kT = \sum_{\alpha=1}^C \sum_{i=1}^{n_\alpha^\phi} \frac{1}{4R_{g\alpha}^2} \int_0^1 ds \left| \frac{d\mathbf{R}_{\alpha i}^\phi(s)}{ds} \right|^2 \quad (1)$$

where $R_{g\alpha}$ is the unperturbed radius of gyration of copolymer species α . For brevity, we will employ the shorthand notation $\sum_{\alpha i} = \sum_{\alpha=1}^C \sum_{i=1}^{n_\alpha^\phi}$

The Van der Waals interactions produce a net attraction between the mesoscale units. In the usual case, chemical units of the same species experience a stronger attraction than dissimilar units. When combined with incompressibility, this results in a net effective repulsion between dissimilar species. This interaction is short-ranged and is approximated to occur at a single point. The energy penalties for dissimilar monomer-monomer and monomer-wall contacts are

$$H_{\phi\phi}/kT = \frac{1}{v_0 \bar{N}} \int d\mathbf{r} \frac{1}{2} \sum_{\alpha, i} \sum_{\beta, j} \hat{\phi}_{\alpha i} \bar{N} \chi_{\alpha i \beta j}^\phi \hat{\phi}_{\beta j} \quad (2)$$

$$H_{\phi\psi}/kT = \frac{1}{v_0 \bar{N}} \int d\mathbf{r} \sum_i \sum_{\beta, j} \psi_i \bar{N} \chi_{i \beta j}^\psi \hat{\phi}_{\beta j} \quad (3)$$

where the volume fraction operator for each monomer species is $\hat{\phi}_{\alpha i} = v_0 N_\alpha^\phi \sum_{j=1}^{n_\alpha^\phi} \int_0^1 ds [\delta(\mathbf{R}_{\alpha j}(s)) \gamma_{\alpha i}(s)]$ and the field $\psi_j(\mathbf{r})$ represents the volume fraction of solid material of type j at the point \mathbf{r} . The strength of the effective repulsion between dissimilar units is given by the Flory χ parameters.

We complete the mesoscale model by constructing a partition function over all physically realizable configurations of the system. The system is isothermal, has a fixed number of mesoscale units, and a fixed volume. Therefore, we construct the partition function in the canonical ensemble.

$$Z = Z_0 \int \prod_{\alpha, \beta, i, j} \mathcal{D}[\mathbf{R}_{\alpha i}^\phi] \delta(\phi_{\beta j} - \hat{\phi}_{\beta j}) \exp(-H/kT) \quad (4)$$

The ensemble sum runs over all possible space curves for each copolymer in the melt with a delta functions that ensures only those distributions that are consistent with the hydrodynamic volume fraction fields are included. The Hamiltonian is $H[\mathbf{R}^\phi(\mathbf{s})] = H_{\phi\phi} + H_{\phi\psi} + H_0$. Note that although this microscopic model explicitly captures the enthalpic and entropic effects associated with copolymers, it does not prevent space curves from crossing each other, and therefore does not explicitly model entanglement.

2.2 Conversion to Field Theoretic Form

We now proceed to convert the mesoscale model to a field theoretic form in which the fundamental degrees of freedom are contained in continuous volume fraction and chemical potential fields. We begin by using the delta functions to replace the volume fraction operators in the interaction terms with their equivalent field values. The interaction terms become

$$H_1/kT = \frac{1}{v_0 \bar{N}} \int d\mathbf{r} \left[\frac{1}{2} \sum_{\alpha,i} \sum_{\beta,j} \phi_{\alpha i} \bar{N} \chi_{\alpha i \beta j}^\phi \phi_{\beta j} + \sum_i \sum_{\beta,j} \psi_i \bar{N} \chi_{i \beta j}^\psi \phi_{\beta j} \right] \quad (5)$$

For each delta functions in Z , we substitute Fourier representations for the monomer volume fractions $\delta(\phi_{\beta j} - \hat{\phi}_{\beta j}) = \int_{-\infty}^{\infty} \mathcal{D}[k_{\beta j}^\phi] \exp \left[\int d\mathbf{r} i k_{\beta j}^\phi (\phi_{\beta j} - \hat{\phi}_{\beta j}) \right]$. For the sake of notational simplicity, we now replace each Fourier mode with field variables that have been rotated in the complex plane and scaled to match the other interactions terms, according to $i k_{\beta j}^\phi = \omega_{\beta j}^\phi / (v_0 \bar{N})$, and the delta functions take the form $\delta(\phi_{\beta j} - \hat{\phi}_{\beta j}) = \int_{-i\infty}^{i\infty} \mathcal{D}[\omega_{\beta j}^\phi] \exp \left[\frac{1}{v_0 \bar{N}} \int d\mathbf{r} \omega_{\beta j}^\phi (\phi_{\beta j} - \hat{\phi}_{\beta j}) \right]$.

For each copolymer species α , we gather together all the quantities that depend explicitly on $\mathbf{R}_{\alpha i}^\phi$ into a single term.

$$(Q_\alpha^\phi)^{n_\alpha^\phi} = \int \prod_{i=1}^{n_\alpha^\phi} \mathcal{D}[\mathbf{R}_{\alpha i}] \exp \left[- \sum_{i=1}^{M_\alpha^\phi} \frac{1}{v_0 \bar{N}} \int d\mathbf{r} \omega_{\alpha i}^\phi \hat{\phi}_{\alpha i} - \sum_{i=1}^{n_\alpha^\phi} \frac{1}{4R_{g\alpha}^2} \int_0^1 ds \left| \frac{d\mathbf{R}_{\alpha i}}{ds} \right|^2 \right] \quad (6)$$

Because each copolymer is indistinguishable from others of the same species, when we insert the definition of the volume fraction operator into Eq. 6, it factors into a product of n_α^ϕ identical single chain partition functions.

$$Q_\alpha^\phi = Q_0 \int \mathcal{D}[\mathbf{R}] \exp \left[- \int_0^1 ds \left(\frac{N_\alpha}{\bar{N}} \omega_\alpha(s) + \frac{1}{4R_{g\alpha}^2} \left| \frac{d\mathbf{R}_{\alpha i}}{ds} \right|^2 \right) \right] \quad (7)$$

where we have defined $\omega_\alpha(s) = \sum_{i=1}^{M_\alpha^\phi} \omega_{\alpha i}^\phi(s) \gamma_{\alpha i}(s)$. As usual, this sum over space curves can be converted into a volume integral over a propagator in a manner analogous to that employed by Feynman and Kac[11] in their path integral formulation of quantum mechanics, as expressed by $Q = \frac{1}{V} \int d\mathbf{r} q_\alpha(\mathbf{r}, s) q_\alpha^\dagger(\mathbf{r}, s)$. The propagator and co-propagator are evaluated by numerically solving the differential equations with initial conditions $q_\alpha(\mathbf{r}, 0) = 1$ and $q_\alpha^\dagger(\mathbf{r}, 1) = 1$.

$$\partial_s q_\alpha(\mathbf{r}, s) = +R_{\alpha g}^2 \nabla^2 q_\alpha(\mathbf{r}, s) - (N_\alpha/\bar{N}) \omega_\alpha(s) q_\alpha(\mathbf{r}, s) \quad (8)$$

$$\partial_s q_\alpha^\dagger(\mathbf{r}, s) = -R_{\alpha g}^2 \nabla^2 q_\alpha^\dagger(\mathbf{r}, s) + (N_\alpha/\bar{N}) \omega_\alpha(s) q_\alpha^\dagger(\mathbf{r}, s) \quad (9)$$

At this point, we have converted the original partition function into an ensemble sum over all possible conjugate field configurations $Z = Z_0 \int \mathcal{D}\omega_{\alpha i}^\phi \exp(\mathcal{F}[\omega, \phi, \psi]/kT)$ with an effective Hamiltonian that is a functional of the chemical potential fields and the volume fraction fields. This effective hamiltonian can be expressed $\mathcal{F} = U - TS$ where the enthalpy and entropy of the system are given by the relations

$$U/kT = \frac{1}{v_0 \bar{N}} \int d\mathbf{r} \left[\frac{1}{2} \sum_{\alpha, i} \sum_{\beta, j} \phi_{\alpha i} \bar{N} \chi_{\alpha i \beta j}^\phi \phi_{\beta j} + \sum_i \sum_{\beta, j} \psi_i \bar{N} \chi_{i \beta j}^\psi \phi_{\beta j} \right] \quad (10)$$

$$S/k = \sum_\alpha n_\alpha^\phi \ln Q_\alpha + \frac{1}{v_0 \bar{N}} \int d\mathbf{r} \sum_{\alpha, i} \phi_{\alpha i} \omega_{\alpha i}^\phi \quad (11)$$

2.3 Mean Field Approximation

Since we do not know how to evaluate the partition function analytically, it must be numerically sampled or analytically approximated. To this end, we perform a steepest descent analysis to obtain a mean field approximation Z . The free energy is then approximated by the value of the effective hamiltonian of the mean field state $F \approx \mathcal{F}[\omega^*]$. To find the mean field state, we extremize \mathcal{F} with respect to the conjugate chemical potentials $\omega_{\alpha i}^\phi$. The resulting equations are the local thermodynamic equilibrium (LTE) conditions,

$$\left. \frac{\delta \mathcal{F}}{\delta \omega_{\alpha i}^\phi(\mathbf{r})} \right|_{\omega^*} = \frac{kT}{v_0 \bar{N}} (\phi_{\alpha i} - \tilde{\phi}_{\alpha i}) = 0 \quad (12)$$

where the auxiliary monomer volume fractions are defined to be $\tilde{\phi}_{\alpha i} = -v_0 \bar{N} n_\alpha^\phi \frac{\delta \ln Q_\alpha}{\delta \omega_{\alpha i}^\phi(\mathbf{r})}$. These auxiliary monomer fractions may also be expressed in terms of the propagators, $\tilde{\phi}_{\alpha i}(\mathbf{r}) = \frac{f_\alpha^c}{Q_\alpha} \int_0^1 ds q_\alpha(\mathbf{r}, s) q_\alpha^\dagger(\mathbf{r}, s) \gamma_{\alpha i}(s)$ where the quantity $f_\alpha^c =$

$n_\alpha^\phi N_\alpha (v_0/V)$ is the volume fraction occupied by all copolymers of species α in the melt.

The LTE equation (12) represents a set of highly nonlinear conditions that specify the conjugate potential fields $\omega_{\alpha i}^\phi$ as a function of the volume fraction fields $\phi_{\alpha i}$. Once the the LTE conditions have been satisfied, we can compute the non-equilibrium chemical potentials which are derived from the functional derivatives of the free energy with respect to the volume fraction fields.

$$\mu_i^\psi(\mathbf{r}) = \frac{\delta \mathcal{F}}{\delta \psi_i(\mathbf{r})} \Bigg|_{\omega^*} = \frac{kT}{\bar{N}v_0} \sum_{\beta j} \bar{N} \chi_{i\beta j}^\psi \phi_{\beta j} \quad (13)$$

$$\mu_{\alpha i}^\phi(\mathbf{r}) = \frac{\delta \mathcal{F}}{\delta \phi_{\alpha i}(\mathbf{r})} \Bigg|_{\omega^*} = \frac{kT}{\bar{N}v_0} \left[\sum_{\beta j} \bar{N} \chi_{\alpha i \beta j}^\phi \phi_{\beta j} + \sum_k \bar{N} \chi_{k \alpha i}^\psi \psi_k - \omega_{\alpha i}^\phi \right] \quad (14)$$

3 Multiple Fluid Model With Walls

In this section, we derive a hydrodynamic model that is appropriate for modeling transport of multiple viscoelastic fluids in the presence of rigid channel walls. We briefly review Rayleigh's variational principle, used in [12] to obtain the two fluid model for polymer solutions and blends and apply the same procedure to derive the multi-fluid model.

3.1 Review of Rayleigh's Variational Principle

For systems that are not too far out of equilibrium, the theory of irreversible thermodynamics makes the approximation that the generalized velocities in the system are linearly related to the generalized forces by $\frac{dx_i}{dt} = -\sum_j L_{ij} \frac{\partial F}{\partial x_j}$ where x_i are the generalized systems variables, and L_{ij} are Onsager coefficients. For cases where the inverse of the kinetic Onsager coefficient matrix is defined, this relationship may be re-expressed as $\frac{\partial F}{\partial x_i} + \sum_j L_{ij}^{-1} \frac{dx_j}{dt} = 0$. This equation of motion may be equally well expressed in terms of a variational principle in the generalized velocities $\delta R = 0$ where $R = \sum_i \frac{\partial F}{\partial x_i} \dot{x}_i + \frac{1}{2} \sum_{i,j} L_{ij}^{-1} \dot{x}_i \dot{x}_j$. The two terms in the Rayleigh functional $R = \dot{F} + \frac{1}{2}W$ can interpreted as the total change in free energy \dot{F} and an energy dissipation function W .

3.2 Multi-fluid Model Derivation

For the system we are considering, the total change in free energy is

$$\dot{F} = \int d\mathbf{r} \left[\sum_{\alpha=1}^C \sum_{i=1}^{M_{\alpha}^{\phi}} \frac{\delta F}{\delta \phi_{\alpha i}(\mathbf{r})} \dot{\phi}_{\alpha i}(\mathbf{r}) + \sum_{j=1}^{M^{\psi}} \frac{\delta F}{\delta \psi_j(\mathbf{r})} \dot{\psi}_j(\mathbf{r}) \right] \quad (15)$$

In the absence of chemical reactions, each component is conserved, so the monomer fields obey $\dot{\phi}_{\alpha i} = -\nabla \cdot \phi_{\alpha i} \mathbf{v}_{\alpha i}^{\phi}$ and the solid fields obey $\dot{\psi}_j = -\nabla \cdot \psi_j \mathbf{v}_j^{\psi}$. Mass is also conserved in the absence of sources or sinks, which is enforced by the divergence free condition $\nabla \cdot \mathbf{v} = 0$ where $\mathbf{v} = \sum_{\alpha i} \phi_{\alpha i} \mathbf{v}_{\alpha i} + \sum_j \psi_j \mathbf{v}_j^{\psi}$ is the mean velocity of all materials. The total change in free energy can be written in terms of the monomer velocities $\mathbf{v}_{\alpha i}^{\phi}$ and the rigid wall velocities \mathbf{v}_j^{ψ} as

$$\dot{F} = \int d\mathbf{r} \left[- \sum_{\alpha i} \mu_{\alpha i}^{\phi} \nabla \cdot \phi_{\alpha i} \mathbf{v}_{\alpha i}^{\phi} - \sum_j \mu_j^{\psi} \nabla \cdot \psi_j \mathbf{v}_j^{\psi} \right] \quad (16)$$

To construct W , we note that energy is dissipated due to friction between the monomers and the entangled polymer network $\zeta_i^{\phi} (\mathbf{v}_{\alpha i}^{\phi} - \mathbf{v}_T)^2$, by friction between the solid material and the network $\zeta_j^{\psi} (\mathbf{v}_j^{\psi} - \mathbf{v}_T)^2$, and by elastic deformation of the network $\boldsymbol{\sigma} : \nabla \mathbf{v}_T$. Energy is also added to the system by the externally driven rigid walls $\mathbf{f}_j^{\psi} \cdot \mathbf{v}_j^{\psi}$ and by the presence of body forces acting on the bulk of the fluid, $\mathbf{f}_{\alpha i}^{\phi} \cdot \mathbf{v}_{\alpha i}^{\phi}$. Therefore, we construct a dissipation function of the form

$$\frac{W}{2} = \int d\mathbf{r} \left[\sum_{\alpha i} \left(\frac{1}{2} \zeta_{\alpha i}^{\phi} (\mathbf{v}_{\alpha i}^{\phi} - \mathbf{v}_T)^2 - \mathbf{f}_{\alpha i}^{\phi} \cdot \mathbf{v}_{\alpha i}^{\phi} \right) + \sum_j \left(\frac{1}{2} \zeta_j^{\psi} (\mathbf{v}_j^{\psi} - \mathbf{v}_T)^2 - \mathbf{f}_j^{\psi} \cdot \mathbf{v}_j^{\psi} \right) + \boldsymbol{\sigma} : \nabla \mathbf{v}_T \right] \quad (17)$$

The velocity field describing the motion of the entangled polymer network is called the tube velocity $\mathbf{v}_T = \sum_{\alpha i} \alpha_{\alpha i}^{\phi} \mathbf{v}_{\alpha i}^{\phi} + \sum_j \alpha_j^{\psi} \mathbf{v}_j$ which is a rheological mean velocity where each component is weighted by the stress division parameters. The tube velocity \mathbf{v}_T may also be expressed in terms of the mean velocity \mathbf{v} and the relative velocities $\mathbf{w}_{\alpha i}^{\phi} = \mathbf{v}_{\alpha i}^{\phi} - \mathbf{v}_T$ using the following relation.

$$\mathbf{v}_T = \frac{\sum_i (\alpha_i^{\phi} - \phi_i) \mathbf{w}_i^{\phi} + \sum_j (\alpha_j^{\psi} - \psi_j) \mathbf{v}_j^{\psi} + \mathbf{v}}{1 - \sum_i (\alpha_i^{\phi} - \phi_i)} \quad (18)$$

In the case of a dynamically symmetric system, the tube velocity reduces to the mean velocity. Solving the momentum balance condition $0 = \sum_{\alpha i} \zeta_{\alpha i}^{\phi} (\mathbf{v}_{\alpha i}^{\phi} -$

$\mathbf{v}_T) + \sum_j \zeta_j^\psi (\mathbf{v}_j^\psi - \mathbf{v}_T)$ allows us to identify the stress division parameters as $\alpha_{\alpha i}^\phi = \zeta_{\alpha i}^\phi / \zeta$ and $\alpha_i^\psi = \zeta_j^\psi / \zeta$ where the sum of the friction coefficients is $\zeta = \sum_{\alpha i} \zeta_{\alpha i}^\phi + \sum_j \zeta_j^\psi$. In this paper, we assume the friction coefficients have the form $\zeta_{\alpha i}^\phi = \zeta_{0i}^\phi (N_\alpha / N_{e\alpha}) (n_\alpha^\phi / V) \phi_{\alpha i}$ and $\zeta_j^\psi = \zeta_{0j}^\psi (n_j^\psi / V) \psi_j / \Phi$. As discussed in [13] the wall friction coefficient is taken to be inversely proportional to the porosity of the material $\Phi = \sum_{\alpha i} \phi_{\alpha i} = 1.0 - \sum_j \psi_j$. For this discussion, we assume the body forces take the form $\mathbf{f}_{\alpha i}^\phi = \mathbf{f}_e \phi_{\alpha i}$ where \mathbf{f}_e is a constant, externally applied force (such as a uniform gravitational field.)

Equations of motion for each component are obtained by appending the divergence free condition to the Rayleigh functional $R = \dot{F} + \frac{1}{2}W - p(\nabla \cdot \mathbf{v})$ and then extremizing it with respect to the velocity fields, $\frac{\delta R}{\delta \mathbf{v}_{\alpha i}^\phi} = 0$ and $\frac{\delta R}{\delta \mathbf{v}_j^\psi} = 0$. The full Rayleigh functional (with implied summation over repeated indices) is

$$R = \int d\mathbf{r} \left[-\mu_{\alpha i}^\phi \nabla \cdot \phi_{\alpha i} \mathbf{v}_{\alpha i}^\phi - \mu_j^\psi \nabla \cdot \psi_j \mathbf{v}_j^\psi - p(\nabla \cdot \mathbf{v}) + \boldsymbol{\sigma} : \nabla \mathbf{v}_T \right. \\ \left. + \frac{1}{2} \zeta_{\alpha i}^\phi (\mathbf{v}_{\alpha i}^\phi - \mathbf{v}_T)^2 + \frac{1}{2} \zeta_j^\psi (\mathbf{v}_j^\psi - \mathbf{v}_T)^2 - \mathbf{f}_j^\psi \cdot \mathbf{v}_j^\psi - \mathbf{f}_{\alpha i}^\phi \cdot \mathbf{v}_{\alpha i}^\phi \right] \quad (19)$$

which produces the following equations of motion,

$$0 = \phi_{\alpha i} \nabla \mu_{\alpha i}^\phi + \phi_{\alpha i} \nabla p - \alpha_{\alpha i}^\phi \nabla \cdot \boldsymbol{\sigma} + \zeta_{\alpha i}^\phi (\mathbf{v}_{\alpha i}^\phi - \mathbf{v}_T) - \phi_{\alpha i} \mathbf{f}_e \quad (20)$$

$$0 = \psi_j \nabla \mu_j^\psi + \psi_j \nabla p - \alpha_j^\psi \nabla \cdot \boldsymbol{\sigma} + \zeta_j^\psi (\mathbf{v}_j^\psi - \mathbf{v}_T) - \mathbf{f}_j^\psi \quad (21)$$

Eq. (20) can be solved for the velocity of each fluid relative to the elastic polymer network $\mathbf{w}_{\alpha i}^\phi = \mathbf{v}_{\alpha i}^\phi - \mathbf{v}_T$, and Eq.(21) gives the local forces $\mathbf{f}_j^\psi(\mathbf{r})$ that must be applied to maintain the specified wall motion $\mathbf{v}_j^\psi(\mathbf{r})$.

$$\mathbf{w}_{\alpha i}^\phi = \frac{1}{\zeta_{\alpha i}^\phi} \left[\alpha_{\alpha i}^\phi \nabla \cdot \boldsymbol{\sigma} - \phi_{\alpha i} \nabla \mu_{\alpha i}^\phi - \phi_{\alpha i} \nabla p + \phi_{\alpha i} \mathbf{f}_e \right] \quad (22)$$

$$\mathbf{f}_j^\psi = \psi_j \nabla \mu_j^\psi + \psi_j \nabla p - \alpha_j^\psi \nabla \cdot \boldsymbol{\sigma} + \zeta_j^\psi (\mathbf{v}_j^\psi - \mathbf{v}_T) \quad (23)$$

Eq. (23) states that the wall force must be sufficient to overcome the osmotic pressure, the hydrostatic pressure, the viscoelastic forces and friction with the copolymer melt. When we sum Eq. (20) and Eq. (21) over all components, we get the momentum balance condition

$$0 = \nabla \pi + \nabla p - \nabla \cdot \boldsymbol{\sigma} - \mathbf{f}^\psi - \Phi \mathbf{f}_e \quad (24)$$

This condition is the transport equation for the total momentum in the limit of zero Reynolds number which together with the divergence free condition implicitly specifies \mathbf{v} . The total osmotic pressure is defined as $\nabla \pi = \sum_{\alpha i} \phi_{\alpha i} \nabla \mu_{\alpha i}^\phi +$

$\sum_j \psi_j \mu_j^\psi$ and the net external force exerted by the walls is $\mathbf{f}^\psi = \sum_j \mathbf{f}_j^\psi$. The total body force acting on the fluid is $\mathbf{f}^\phi = \sum_{\alpha i} \mathbf{f}_{\alpha i}^\phi = \Phi \mathbf{f}_e$.

3.3 Viscoelastic Constitutive Equation

The constitutive equations (25) and (26) measure the bulk elastic stresses $\boldsymbol{\sigma}_{\alpha i}^b$ and shear elastic stresses $\boldsymbol{\sigma}_{\alpha i}^s$ that are induced by deformations of each entangled polymeric component.

$$\dot{\boldsymbol{\sigma}}_{\alpha i}^s = G_{\alpha i} \kappa_T - \boldsymbol{\sigma}_{\alpha i}^s / \tau_\alpha \quad (25)$$

$$\dot{\boldsymbol{\sigma}}_{\alpha i}^b = K_{\alpha i} (\nabla \cdot \mathbf{v}_T) \boldsymbol{\delta} - \boldsymbol{\sigma}_{\alpha i}^b / \tau_\alpha \quad (26)$$

Although there are many possible constitutive equations, we have chosen to employ an Oldroyd-B model for its simplicity. The total viscoelastic force is the sum of the elastic forces contributed by each polymeric component and a dissipative viscous force. $\nabla \cdot \boldsymbol{\sigma} = \sum_{\alpha i} (\nabla \cdot \boldsymbol{\sigma}_{\alpha i}^s + \nabla \cdot \boldsymbol{\sigma}_{\alpha i}^b) + \eta_s \nabla^2 \mathbf{v}_T$. This model allows us to study a purely viscous fluid ($G_{\alpha i} = K_{\alpha i} = 0$), a purely viscoelastic melt ($\eta_s = 0$), or anything in-between. The derivatives in Eq. (25) and Eq. (26) are upper convected time derivatives, $\dot{\boldsymbol{\sigma}} = \partial_t \boldsymbol{\sigma} + \mathbf{v}_T \cdot \nabla \boldsymbol{\sigma} - \boldsymbol{\sigma} \cdot \nabla \mathbf{v}_T - (\nabla \mathbf{v}_T)^\dagger \cdot \boldsymbol{\sigma}$, and the shear strain rate tensor is $\kappa_T^{ij} = \partial_i v_T^j + \partial_j v_T^i - \frac{2}{d} (\nabla \cdot \mathbf{v}_T) \delta_{ij}$. The concentration dependent volumetric moduli $K_{\alpha i}$ and shear moduli $G_{\alpha i}$ measure stresses imposed on a single component by the applied strains. Following Tanaka's example [14], we employ moduli of the form $G_{\alpha i}(\phi) = G_{0\alpha i} \phi_{\alpha i}^2$ and $K_{\alpha i}(\phi) = K_{0\alpha i} \theta(\phi_{\alpha i} - f_{\alpha i})$. For simulations with large elastic strains, the constitutive equation may be replaced with a more sophisticated phenomenological model or one based upon the SCFT microphysics [15].

4 Nondimensionalization

In order to convert the equations to dimensionless form, we choose the characteristic energy to be the thermal energy $e_c = kT$, the characteristic velocity to be the convective velocity $v_c = l_c/t_c$, and the characteristic length-scale to be the average radius of gyration in the system $l_c = \bar{R}_g = b \sqrt{\bar{N}/2d}$ where b is the statistical segment length of a mesoscale chemical unit and d is the dimension of the system.

Inserting these definitions, the propagator and copropagators equations may be expressed as

$$\partial_s q_\alpha(\mathbf{r}, s) = +\lambda_\alpha \left[\hat{\nabla}^2 q_\alpha(\mathbf{r}, s) - \omega_\alpha(s) q_\alpha(\mathbf{r}, s) \right] \quad (27)$$

$$\partial_s q_\alpha^\dagger(\mathbf{r}, s) = -\lambda_\alpha \left[\hat{\nabla}^2 q_\alpha^\dagger(\mathbf{r}, s) - \omega_\alpha(s) q_\alpha^\dagger(\mathbf{r}, s) \right] \quad (28)$$

where $\hat{\nabla} = (1/l_c)\nabla$ and $\lambda_\alpha = N_\alpha/\bar{N}$. Similarly, we choose to define $\mu_c = \frac{kT}{v_0}$ so that the dimensionless chemical potentials are defined as

$$\hat{\mu}_i^\psi(\mathbf{r}) = \sum_{\beta j} \chi_{i\beta j}^\psi \phi_{\beta j} \quad (29)$$

$$\hat{\mu}_{\alpha i}^\phi(\mathbf{r}) = \sum_{\beta j} \chi_{\alpha i \beta j}^\phi \phi_{\beta j} + \sum_k \chi_{k \alpha i}^\psi \psi_k - \omega_{\alpha i}^\phi / \bar{N} \quad (30)$$

Applying these same conventions to the hydrodynamic model gives the dimensionless incompressibility condition and monomer transport equations.

$$0 = \hat{\nabla} \cdot \hat{\mathbf{v}} \quad (31)$$

$$\hat{\partial}_t \phi_{\alpha i} = -\hat{\nabla} \cdot \phi_{\alpha i} \hat{\mathbf{v}}_{\alpha i}^\phi \quad (32)$$

$$\hat{\partial}_t \psi_i = -\hat{\nabla} \cdot \psi_i \hat{\mathbf{v}}_i^\psi \quad (33)$$

Furthermore, we define the elastic stresses in terms of the largest shear modulus in the system $\sigma_c = \max(G_{\alpha i})$ and the characteristic time is chosen to be the largest reptative disentanglement time $t_c = \max(\tau_\alpha)$. With these choices, the constitutive equations in dimensionless form are

$$\dot{\hat{\boldsymbol{\sigma}}}_{\alpha i}^s = \hat{G}_{\alpha i} \phi_{\alpha i}^2 \hat{\kappa}_T - \hat{\boldsymbol{\sigma}}_{\alpha i}^s / \hat{\tau}_\alpha \quad (34)$$

$$\dot{\hat{\boldsymbol{\sigma}}}_{\alpha i}^b = \hat{K}_{\alpha i} \theta(\phi_{\alpha i} - f_{\alpha i}) (\hat{\nabla} \cdot \hat{\mathbf{v}}_T) \boldsymbol{\delta} - \hat{\boldsymbol{\sigma}}_{\alpha i}^b / \hat{\tau}_\alpha \quad (35)$$

where the dimensionless shear moduli are $\hat{G}_{\alpha i} = G_{\alpha i}/\sigma_c$, the dimensionless bulk moduli are $\hat{K}_{\alpha i} = K_{\alpha i}/\sigma_c$, and the dimensionless relaxation times are $\hat{\tau}_\alpha = \tau_\alpha/t_c$.

Following convention, we scale each term in the momentum balance equation by the characteristic viscoelastic force $f_c = \eta_c v_c/l_c^2$, where $\eta_c = \sigma_c t_c$, which gives

$$0 = \text{Ca}^{-1} \hat{\nabla} \hat{\pi} + \hat{\nabla} \hat{p} - \hat{\nabla} \cdot \hat{\boldsymbol{\sigma}} - \hat{\mathbf{f}}^\psi - \Phi \hat{\mathbf{f}}_e \quad (36)$$

where $\text{Ca} = \frac{\eta_c v_c}{l_c \mu_c}$ is the Capillary number. Similarly, the equations for the relative velocity field and wall forces become

$$\Gamma \hat{\zeta}_{\alpha i}^\phi \hat{\mathbf{w}}_{\alpha i}^\phi = -\text{Ca}^{-1} \phi_{\alpha i} \hat{\nabla} \hat{\mu}_{\alpha i}^\phi - \phi_{\alpha i} \hat{\nabla} \hat{p} + \alpha_{\alpha i}^\phi \hat{\nabla} \cdot \hat{\boldsymbol{\sigma}} + \phi_{\alpha i} \hat{\mathbf{f}}_e \quad (37)$$

$$\hat{\mathbf{f}}_j^\psi = \text{Ca}^{-1} \psi_j \hat{\nabla} \hat{\mu}_j^\psi + \psi_j \hat{\nabla} \hat{p} - \alpha_j^\psi \hat{\nabla} \cdot \hat{\boldsymbol{\sigma}} + \Gamma \hat{\zeta}_j^\psi (\hat{\mathbf{v}}_j^\psi - \hat{\mathbf{v}}_T) \quad (38)$$

where $\Gamma = \frac{\zeta_c l_c^2}{\eta_c}$ is a dimensionless friction factor and $\zeta_c = \min(\zeta_{0i})$ is the smallest monomer friction coefficient. In the subsequent discussion, we omit the hats from the dimensionless quantities for convenience.

5 Numerical Method

The system is spatially discretized as an array of equally spaced Fourier collocation points. All spatial derivatives are calculated pseudo-spectrally in Fourier space and then transformed to real space using freely distributed parallel FFTW-MPI routines. This approach allows us to resolve sharp interfaces between neighboring phases with a minimum number of grid-points while enabling a fast, parallel implementation. Simulations are performed in a periodic domain in either two or three dimensions and non-periodic channels are approximated by employing an appropriate set of rigid-wall fields. The wall wetting conditions are implicitly specified by the energetic interactions between the fluid and wall fields, $H_{\phi\psi}$. This approach is a diffuse interface method in that boundaries between adjacent polymer phases are explicitly resolved by several grid points, and surface tension between neighboring phases results from the energetic penalty that occurs where two materials come in contact, encoded in $H_{\phi\phi}$.

5.1 Method Overview

The numerical solution of the governing equations consists of the following major steps.

- (1) *Thermodynamic Iteration:* Solve for chemical potential fields μ^ϕ and μ^ψ that are consistent with the non-equilibrium volume fraction fields ϕ and ψ by iteratively searching for a state that satisfies the local thermodynamic equilibrium (LTE) conditions at each collocation point.
- (2) *Hydrodynamic Iteration:* Obtain velocities \mathbf{v} , pressures p , and viscoelastic stresses $\boldsymbol{\sigma}$ that simultaneously satisfy incompressibility, no-flow and no-slip boundary conditions, and the zero Reynolds number momentum balance condition. This is accomplished using a pseudo-time evolution that iterates until a steady state is achieved. A penalization method is employed to satisfy the wall boundary conditions, and a projection method is employed to enforce incompressibility.

(3) *Volume Fraction Transport:* Use the updated velocity fields to transport the volume fractions ϕ and ψ in a flux conserving manner.

In the following sections, the quantity Δt is defined to be the time increment of the outer loop while h represents the size of the hydrodynamic pseudo-time step. Similarly, the superscript $[n]$ counts iterations of the main loop, and $[j]$ counts iterations of the inner, steady-state loops. Also, the Fourier transform of a quantity x is represented by $\tilde{x} = \mathcal{F}(x)$ and the inverse transform is $x = \mathcal{F}^{-1}(\tilde{x})$.

5.2 Thermodynamic Implementation

The thermodynamic model is responsible for producing a set of non-equilibrium chemical potential fields μ^ϕ and μ^ψ that are consistent with the distribution of volume fraction fields ϕ and ψ at each time step. It accomplishes this by iteratively searching for a set of conjugate chemical potentials ω that satisfy the mean field, local equilibrium conditions. The procedure begins by using the conjugate potentials from the previous time step as an estimate for the new potentials $\omega_{\alpha i}^{\phi[j]}$, which it employs to solve the propagator equations (27) and (28). The solution of these equations is computationally expensive and it is important to do so as efficiently as possible. To that end, we employ the pseudo-spectral, operator splitting method developed in [16], which is unconditionally stable in s . The propagators are initialized with $q_\alpha(\mathbf{r}, 0) = 1$, and the copropagators are initialized with $q_\alpha^\dagger(\mathbf{r}, 1) = 1$. The modified diffusion equations are then solved as follows,

$$q_\alpha(\mathbf{r}, s + \Delta s) = e^{-\omega_\alpha \lambda_\alpha \Delta s / 2} \mathcal{F}^{-1} \left[e^{-\lambda_\alpha \Delta s k^2} \mathcal{F} \left[e^{-\omega_\alpha \lambda_\alpha \Delta s / 2} q_\alpha(\mathbf{r}, s) \right] \right] \quad (39)$$

$$q_\alpha^\dagger(\mathbf{r}, s - \Delta s) = e^{-\omega_\alpha \lambda_\alpha \Delta s / 2} \mathcal{F}^{-1} \left[e^{-\lambda_\alpha \Delta s k^2} \mathcal{F} \left[e^{-\omega_\alpha \lambda_\alpha \Delta s / 2} q_\alpha^\dagger(\mathbf{r}, s) \right] \right] \quad (40)$$

where the effective conjugate potential at index s is $\omega_\alpha(\mathbf{r}, s) = \sum \omega_{\alpha i}^{\phi[j]}(\mathbf{r}) \gamma_{\alpha i}(s)$.

The partition function for each copolymer chain is computed by averaging over the entire simulation domain $Q_\alpha = \frac{1}{V} \int q_\alpha(\mathbf{r}, 1)$ and the auxilliary volume fraction fields are computed by quadrature along the polymerization index, $\tilde{\phi}_{\alpha i}(\mathbf{r}) = \frac{f}{Q_\alpha} \int_0^1 ds q_\alpha(\mathbf{r}, s) q_\alpha^\dagger(\mathbf{r}, s) \gamma_{\alpha i}(s)$.

Residual errors are measured by plugging estimated auxiliary volume fractions into the local thermodynamic equilibrium conditions $\varepsilon_{\alpha i}^\omega(\mathbf{r}) = \phi_{\alpha i}(\mathbf{r}) - \tilde{\phi}_{\alpha i}(\mathbf{r})$. In order to find the mean field state, a number of search algorithms may be employed, but we have found simple hill-climbing techniques to be fast and robust. In particular, we use steepest ascent with line minimization as described in [17].

After measuring the residual errors produced by the current conjugate potentials $\varepsilon_{\alpha i}^{\omega[j]}$, a trial step is taken along the gradient of the energy surface $\omega_{\alpha i}^{\phi*}(\mathbf{r}) = \omega_{\alpha i}^{\phi}(\mathbf{r}) + \epsilon \varepsilon_{\alpha i}^{\omega}$, where ϵ is some small adjustable parameter. New residual errors $\varepsilon_{\alpha i}^{\omega*}$ resulting from the update conjugate potentials are then calculated by solving the diffusion equations and computing the auxiliary fields for a second time.

We fit these two points to a parabola to estimate the step size $a = \epsilon \left[\frac{\varepsilon_{11}}{\varepsilon_{11} - \varepsilon_{12}} - 1 \right]$ which will minimize the error along the current search direction, where $\varepsilon_{11} = \frac{1}{V} \int d\mathbf{r} (\varepsilon_{\alpha i}^{\omega})^2$ and $\varepsilon_{12} = \frac{1}{V} \int d\mathbf{r} \varepsilon_{\alpha i}^{\omega} \varepsilon_{\alpha i}^{\omega*}$. We then use this value to advance the fields toward a minimal error solution, $\omega_{\alpha i}^{\phi[j+1]}(r) = \omega_{\alpha i}^{\phi[j]}(r) + (a - \epsilon) \varepsilon_{\alpha i}^{\omega*}(\mathbf{r})$. Once the residual error has converged to within some acceptable tolerance, the chemical potential fields can be calculated using Eqs. (29) and (30).

5.3 Hydrodynamic Implementation

The hydrodynamic model is responsible for calculating the velocities, pressures, and elastic stresses that are produced as a result of internal and external forces on the system. It accomplishes this by iteratively evolving the system in pseudo-time until a steady state (zero Reynolds number) solution is achieved. It then uses these velocity fields to transport each component. The no-flow condition is enforced by an appropriate pressure distribution, which is obtained from a standard projection method. The no slip condition is enforced by friction between each fluid and the walls. By employing a large friction coefficient, relative motion between them is rapidly reduced to zero after a few iterations.

5.3.1 Pseudo-time Iteration

The pseudo-time evolution begins by estimating the elastic stresses using the tube velocity $\mathbf{v}_T^{[j]}$ from the previous iteration. The total elastic stress for each component is defined to be $\boldsymbol{\sigma}_{\alpha i}^e = \boldsymbol{\sigma}_{\alpha i}^s + \boldsymbol{\sigma}_{\alpha i}^b$, which is calculated using a semi-implicit scheme in which the linear terms are handled implicitly and the nonlinear terms are treated explicitly,

$$\boldsymbol{\sigma}_{\alpha i}^{e[j]} = \frac{\boldsymbol{\sigma}_{\alpha i}^{e[n]} + G_{\alpha i} \phi_{\alpha i}^{[n]} \boldsymbol{\kappa}_T^{[j]} + K_{\alpha i} \theta(\phi_{\alpha i}^{[n]} - f_{\alpha i}) \mathcal{F}^{-1} (i\mathbf{k} \cdot \tilde{\mathbf{v}}_T^{[j]}) \boldsymbol{\delta} - \text{UC Terms}}{1 + \Delta t / \tau_{\alpha}} \quad (41)$$

where the upper convected terms are calculated pseudospectrally

$$\text{UC Terms} = \mathcal{F}^{-1} i (\tilde{\mathbf{v}}_T \cdot \mathbf{k} \tilde{\boldsymbol{\sigma}}_{\alpha i} - \mathbf{k} \tilde{\mathbf{v}}_T \cdot \tilde{\boldsymbol{\sigma}}_{\alpha i} - \tilde{\boldsymbol{\sigma}}_{\alpha i} \cdot \tilde{\mathbf{v}}_T \mathbf{k}) \quad (42)$$

as is the shear stress tensor

$$\boldsymbol{\kappa}_T^{[j]} = \mathcal{F}^{-1} i (\mathbf{k} \mathbf{v}_T + \mathbf{v}_T \mathbf{k}) - (2/d) \mathcal{F}^{-1} (i \mathbf{k} \cdot \tilde{\mathbf{v}}_T^{[j]}) \boldsymbol{\delta} \quad (43)$$

The total viscoelastic force is found by summing the elastic forces produced by each component and a dissipative viscous force.

$$\nabla \cdot \boldsymbol{\sigma}^{[j]} = \mathcal{F}^{-1} \left(i \mathbf{k} \cdot \sum_{\alpha i} \tilde{\boldsymbol{\sigma}}_{\alpha i}^{e[j]} - k^2 \eta_s \tilde{\mathbf{v}}_T^{[j]} \right) \quad (44)$$

The relative velocity fields can then be computed using the estimated viscoelastic forces and the pressures produced in the previous iteration,

$$\mathbf{w}^{[j+1]} = \frac{\phi_{\alpha i}^{[n]} \left(f_e^{[n]} - \text{Ca}^{-1} \nabla \mu_{\alpha i}^{\phi [n]} - \nabla p^{[j]} \right) + \alpha_{\alpha i}^{\phi [n]} \nabla \cdot \boldsymbol{\sigma}^{[j]}}{\Gamma \zeta_{\alpha i}^{[n]}} \quad (45)$$

The velocity of each solid object is specified parametrically as a functions of time, and the rigid body motions are converted to a set of wall velocity fields $\mathbf{v}_k^{\psi[n]}$ at each time step. These velocities, together with the other fields calculated thus far enable us to calculate the forces produced by the walls at each point in space.

$$\mathbf{f}_k^{\psi[j]} = \psi_j^{[n]} \left(\text{Ca}^{-1} \nabla \mu_k^{\psi[n]} + \nabla p^{[j]} \right) - \alpha_k^{\psi[n]} \nabla \cdot \boldsymbol{\sigma}^{[j]} + \Gamma \zeta_k^{\psi[n]} (\mathbf{v}_k^{\psi[n]} - \mathbf{v}_T^{[j]}) \quad (46)$$

The momentum balance condition is then satisfied by iteratively reducing the residual error as follows

$$\mathbf{v}^{[j+1]} = \mathbf{v}^{[j]} + h (-\text{Ca}^{-1} \nabla \pi^{[n]} + \nabla \cdot \boldsymbol{\sigma}^{[j]} + \mathbf{f}^{\psi[j]} + \Phi \mathbf{f}_e^{[n]} - \nabla p^{[j+1]}) \quad (47)$$

which can be interpreted as a low Reynolds number evolution of \mathbf{v} in the pseudo-time variable h . Solving for the pressure and velocity fields simultaneously is accomplished using a projection method.

5.4 Projection Method

The projection method obtains the pressures and velocities by solving for an intermediate, compressible velocity field, and then projecting out the incompressible part. We begin by gathering the unknown quantities on the left hand side of the equation

$$v^{[j+1]} + h \nabla p^{[j+1]} = v^{[j]} + h \left(-\text{Ca}^{-1} \nabla \pi^{[n]} + \nabla \cdot \boldsymbol{\sigma}^{[j]} + \mathbf{f}^{\psi[j]} + \Phi \mathbf{f}_e^{[n]} \right) \quad (48)$$

The left hand side can be viewed as the Hobbes decomposition of a single compressible velocity field $\mathbf{v}^* = \mathbf{v}^{[j+1]} + h\nabla p^{[j+1]}$. The value of \mathbf{v}^* is calculated using

$$\mathbf{v}^* = \mathbf{v}^{[j]} + h\mathbf{f}_v \quad (49)$$

where $\mathbf{f}_v = -Ca^{-1}\nabla\pi^{[n]} + \nabla \cdot \boldsymbol{\sigma}^{[j]} + \mathbf{f}^{\psi[j]} + \Phi\mathbf{f}_e^{[n]}$ is the sum of all forces except the pressure gradient. By taking the divergence of \mathbf{v}^* and employing the incompressibility condition $\nabla \cdot \mathbf{v}^{[j+1]} = 0$, we obtain a Poisson equation for the pressure field which may be solved in Fourier space.

$$\nabla^2 p^{[j+1]} = \nabla \cdot \mathbf{v}^* / h \quad (50)$$

$$p^{[j+1]} = -\mathcal{F}^{-1} \left(i\mathbf{k} \cdot \tilde{\mathbf{v}}^* / hk^2 \right) \quad (51)$$

Finally, we can project out the divergence-free portion of the velocity field using the newly computed pressures

$$\mathbf{v}^{[j+1]} = \mathbf{v}^* - h\nabla p^{[j+1]} \quad (52)$$

If the residual errors, $\varepsilon_v = \max \| \mathbf{f}_v - \nabla p \|$ and $\varepsilon_p = \max |\nabla \cdot \mathbf{v}|$, are not within acceptable tolerances, the newly updated $\mathbf{v}^{[j+1]}$ and $p^{[j+1]}$ fields are employed in the next iteration to produce improved estimates.

5.5 Volume Fraction Transport

Once the hydrodynamic iteration has converged, the velocities fields for each component $\mathbf{v}_{\alpha i}^{\phi[n+1]} = \mathbf{v}_T^{[n+1]} + \mathbf{w}_{\alpha i}^{\phi[n+1]}$ are used to transport the volume fraction fields in a flux conserving manner.

$$\phi_{\alpha i}^{[n+1]} = \phi_{\alpha i}^{[n]} + \Delta t \mathcal{F}^{-1} \left(i\mathbf{k} \cdot \mathcal{F} \left(\phi_{\alpha i}^{[n]} \mathbf{v}_{\alpha i}^{\phi[n]} \right) \right) \quad (53)$$

$$\psi_k^{[n+1]} = \psi_k^{[n]} + \Delta t \mathcal{F}^{-1} \left(i\mathbf{k} \cdot \mathcal{F} \left(\psi_k^{[n]} \mathbf{v}_k^{\psi[n]} \right) \right) \quad (54)$$

5.6 Implementation of the Wall Fields

Unbounded chemical potentials would be required in order to produce regions that are completely free of a given component. Therefore, in a manner analogous to other flow penalization techniques [13], we employ slightly porous walls that do not occupy the entire volume at a given point in space. Solid walls with

no slip and no flow boundary conditions are recovered in the limit where the porosity is taken to zero as discussed in [18]. For the simulations presented in this paper, we employ a porosity of $\Phi = 0.01$. Additionally, pseudo-spectral Fourier methods can produce unwanted Gibbs phenomena if the system contains overly sharp interfaces. To prevent this, we apply a Gaussian filter of the form $f(r) = \exp(-r^2/2a)$ to the channel walls to smooth the transition from solid regions to liquid regions in the channel. The characteristic width of the gaussian filter, a , is typically smaller than R_g , and the filter is applied by convolving the two functions in Fourier space, $\psi_{j,\text{smoothed}} = \mathcal{F}^{-1}(\tilde{\psi}_j \tilde{f})$

6 Numerical Results

We validate the method by examining several numerically challenging problems designed to test both its hydrodynamic and thermodynamic capabilities. In each case, we perform a grid refinement study in two dimensions in which we examine the convergence of the method as the mesh size is refined. In addition, we verify that the results are qualitatively consistent with the expected behavior of each system in both two and three dimensions.

6.1 Flow Past a Fixed Sphere

To test the hydrodynamic properties of the model, we examine the benchmark problem of low Reynolds number flow past a fixed spherical obstacle. We generate the pressure driven flow by applying an external force, $\mathbf{f}_e = 0.2$ which drives a melt of homopolymer *A* from top to bottom. Furthermore, we embed a transverse band of incompatible homopolymer *B* to illustrate the manner in which materials are transported by the flow. The strength of the incompatibility for this case is set at $N\chi_{AB} = 8$. The channel is periodic in both directions with dimension $10 \times 20R_g$, and the diameter of the fixed sphere is 40% of the channel width. The sphere interacts neutrally with both materials, $N\chi_{AC} = N\chi_{BC} = 8$. The viscosity is set at $\eta_s = 1.0$, and $G_{\alpha i} = K_{\alpha i} = 0$.

The interaction of the transverse homopolymer band with the fixed spherical obstacle produces an interesting sequence of events in which the homopolymer band wraps around the sphere and is stretched until it ruptures, leaving a layer of *B* in contact with the obstacle. Subsequently, a drop of homopolymer *B* coalesces in the wake of the obstacle, as shown in Fig. 2.

We perform this simulation at three different grids resolutions of 32x64, 48x96, and 64x128, and compare the volume fraction contours produced by each. In

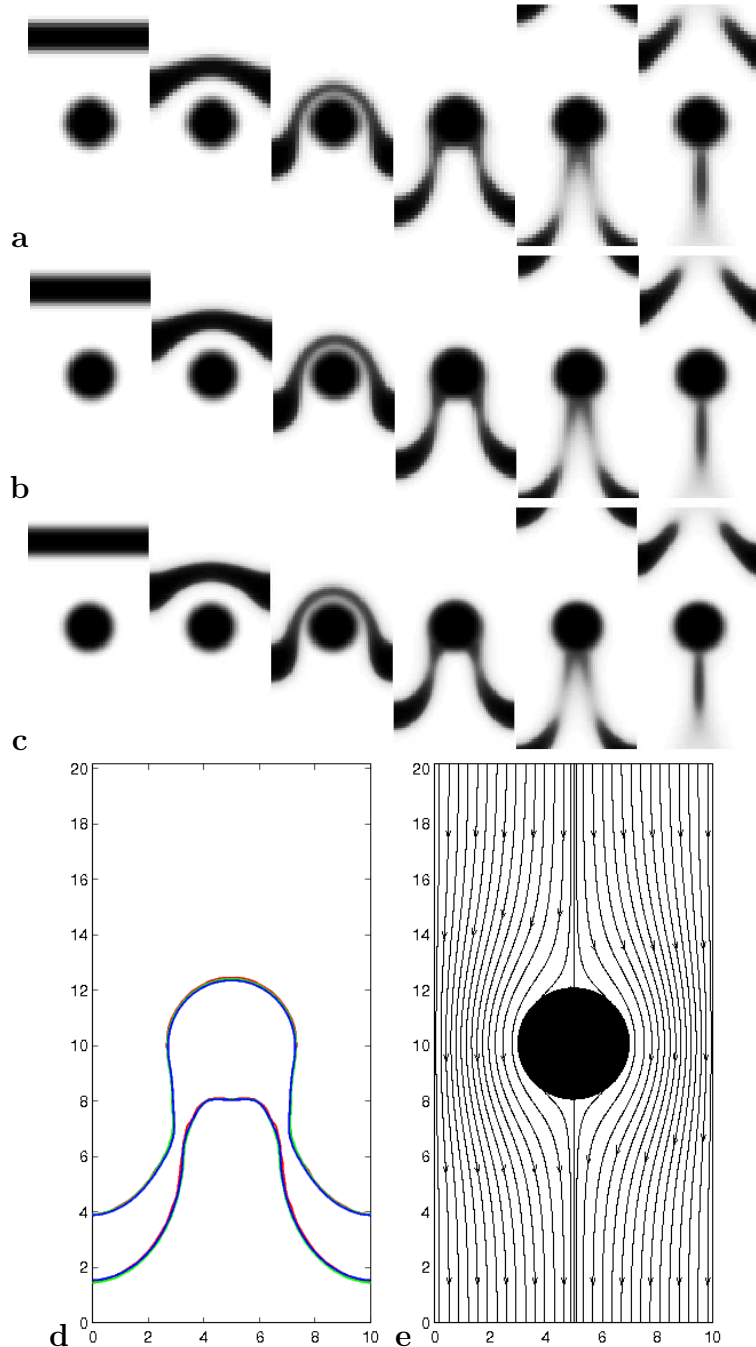


Fig. 2. Typical convergence under grid refinement for the viscous, low Reynolds number flow of a band of homopolymer B past a circular cylinder in a matrix of homopolymer A. Snapshots are taken at $t = 0, 2, 4, 6, 8$, and 10 at three resolutions, (a) 32×64 (red) (b) 48×96 (green) (c) 64×128 (blue). (d) Superposition of homopolymer A interface at all three resolutions at $t=6$. (e) Streamlines of the mean velocity field \mathbf{v}

Fig. 2d the contours of homopolymer A are superimposed at all three resolutions and are found to be nearly identical, indicating that the method converges to a single solution as the simulation mesh is refined. We can character-

ize the flow rate in this experiment by measuring the maximum Weissenberg number $Wi = \tau v_{\max}/L$ where v_{\max} is the maximum mean field velocity, and L is the width of the narrowest portion of the channel. In all three cases, we obtain the same value, $Wi = 0.32$.

In addition, viscous systems in low Reynolds number (creeping) flows are known to produce time-reversible velocity fields. When we plot the streamlines of the mean velocity field \mathbf{v} in Fig. 2e, we observe the expected symmetry about the x axis, and the expected stagnation points at the top and bottom of the obstacle.

6.2 Phase Separation in Diblock Copolymer Melts

In order to validate the thermodynamics, we study phase separation of two quenched diblock copolymer melts. The first melt is constructed from a symmetric block copolymer where both monomer species occupy an equal volume fraction ($f_A = f_B = 0.5$) in the melt, and the interaction strength places the system in the intermediate segregation regime ($N\chi_{AB} = 20$.) The melt is initialized to a well mixed state with an imposed set of small random fluctuations at all frequencies, to break the symmetry.

In Fig. 3 we demonstrate the time evolution of the system and observe that it behaves qualitatively as we would expect. Initially, high frequency modes rapidly decay, and density fluctuations grow exponentially, with the greatest growth occurring for structures at a critical wave number. The fluctuations then saturate, leaving the melt in a highly defect-filled microphase separated state in which the feature size grows over time, until the connectedness of the diblocks prevents further coarsening. The morphological defects persist for long times, and correspond to kinetically trapped states.

In order to study the behavior of the system under grid refinement, we use the same random fluctuation patterns to initialize simulations at grid resolutions of 32×32 , 64×64 , and 128×128 grid points and the periodic system size is fixed at $16 \times 16R_g$. When we overlap the volume fraction contours from all three simulations, we find that the higher resolution runs converge to a single solution as the mesh is refined. However, the lowest resolution predicts a distinctly different defect pattern after the fluctuations saturate. We conclude that at intermediate segregation strengths, two gridpoints per R_g is insufficient to fully resolve the mesoscale structures, but four or eight grid points is adequate.

When we examine the micro-phase separation of an asymmetric diblock, ($f_A = 0.3, f_B = 0.7, N\chi_{AB} = 20$) we see very similar phase separation behavior, except as expected, the minority phase forms a set of isolated drops rather than lamellae, after saturation. When we perform a grid refinement study on this

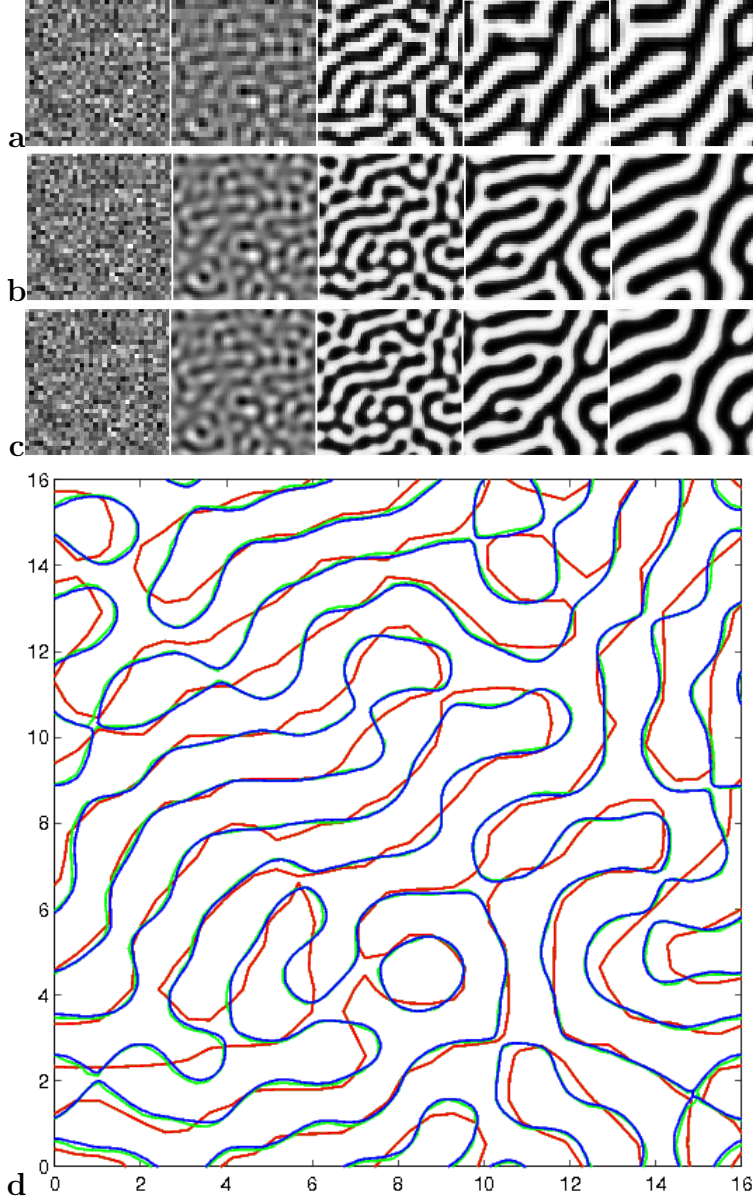


Fig. 3. Typical convergence under grid refinement for a quenched symmetric di-block copolymer melt ($f_A = 0.5, f_B = 0.5, \chi N = 20$). Snapshots where taken at $t = 0, 1, 3, 10$, and 80 for three resolutions (a) 32×32 (red), (b) 64×64 (green), (c) 128×128 (blue). (d) Contours indicate micro-phase boundaries at all three resolutions at $t = 3$.

system, we find that it also converges well as the resolution is increased. However, as before, the lowest resolution run fails to produce the correct pattern of defects. The under-resolved run also incorrectly predicts the subsequent motion of the structures in the later stages of coarsening.

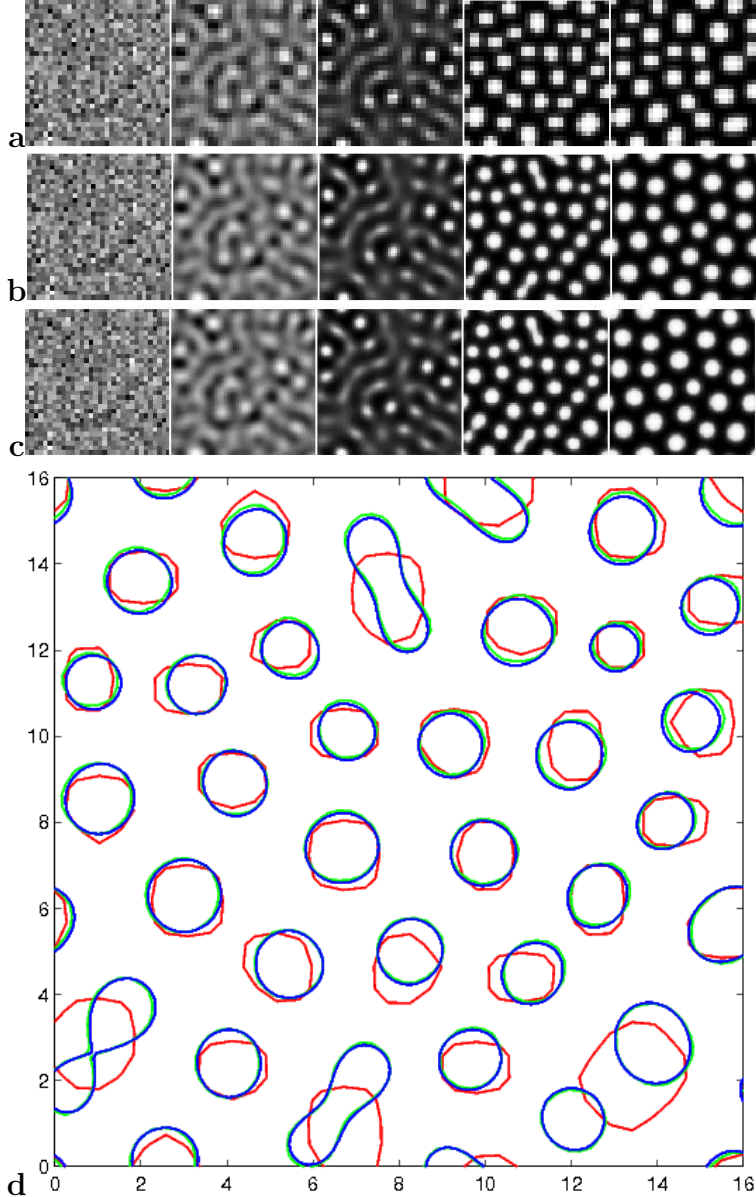


Fig. 4. Typical convergence under grid refinement for a quenched symmetric di-block copolymer melt ($f_A = 0.3, f_B = 0.7, \chi N = 20$). Snapshots were taken at $t = 0, 1, 4, 10$, and 120 for three resolutions (a) 32×32 (red), (b) 64×64 (green), (c) 128×128 (blue). (d) Contours indicate micro-phase boundaries at all three resolutions at $t = 10$.

7 Results in Three Dimensions

Finally, we examine the results of these same test cases in three dimensions

When we examine the flow of a homopolymer band past a fixed sphere in three dimensions, we observe that the results agree qualitatively with the two dimensional simulations, and with expected physical behavior. The three di-

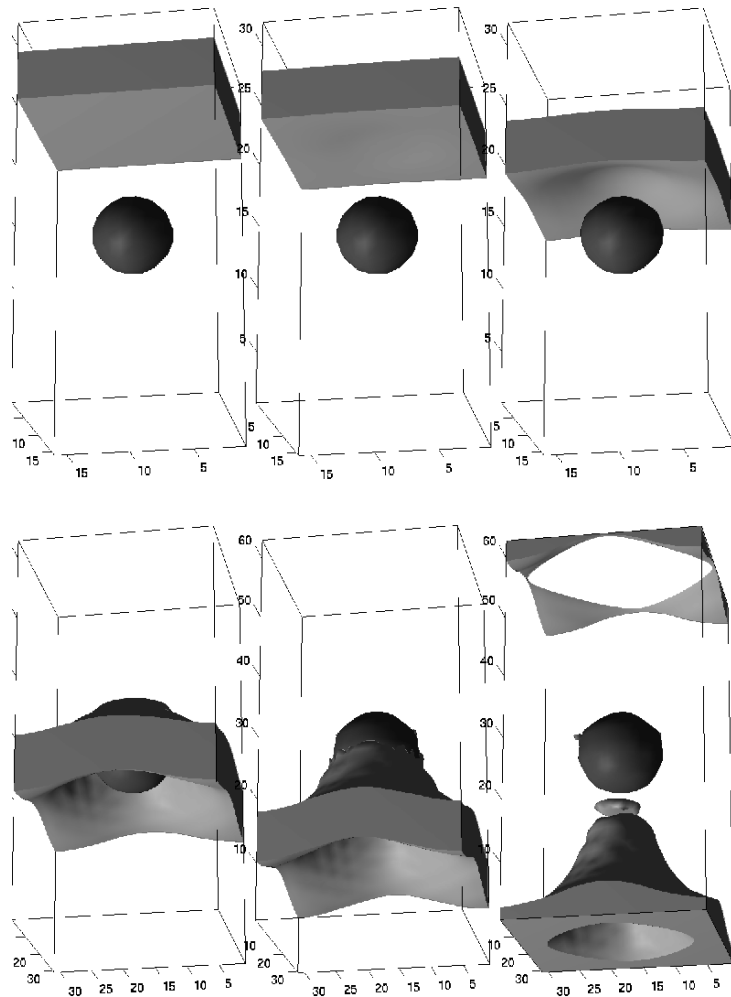


Fig. 5. Flow of a homopolymer band past a fixed sphere in three dimensions

dimensional simulation produces axially symmetric solutions that agree with the two dimensional runs. It is apparent, in three dimensions that the homopolymer band is only punctured, rather than being fully split by the sphere.

We also verify that the diblock copolymer melts produce results that appear to be qualitatively correct in three dimensions, matching the behavior seen in their two dimensional counterparts including: fluctuation growth, saturation, and subsequent evolution in which the defect filled structures coarsen. We note that the symmetric diblock diblock has greater connectivity in the defect filled state than does the asymmetric diblock, as expected.

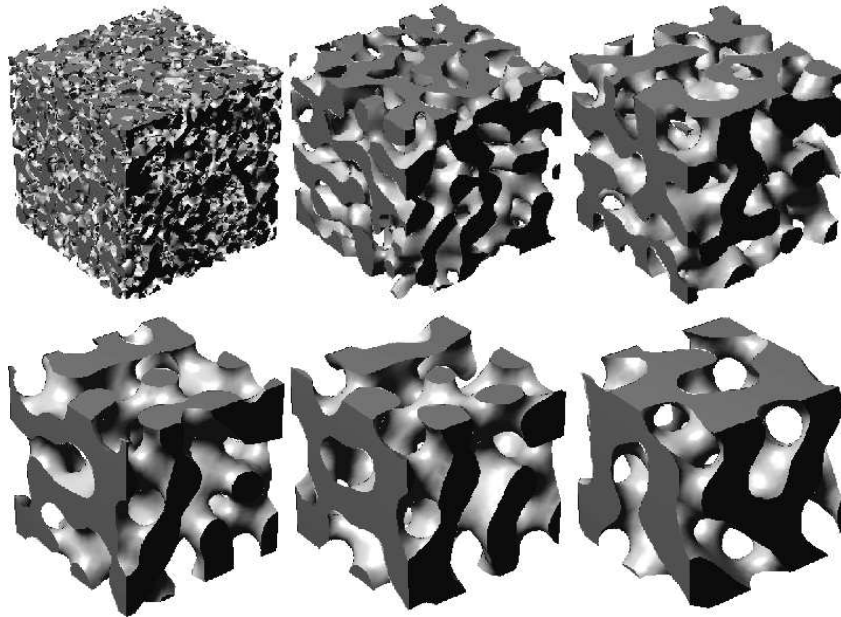


Fig. 6. Phase separation of a symmetric diblock copolymer melt ($f_A = f_B = 0.5, N\chi = 20$) in three dimensions. Snapshots were taken at $t = 0, 1, 5, 10, 20$, and 175.

8 Conclusions

We have constructed a new mesoscale method for simulating inhomogeneous copolymer melts in hydrodynamic flows. The method represents a significant

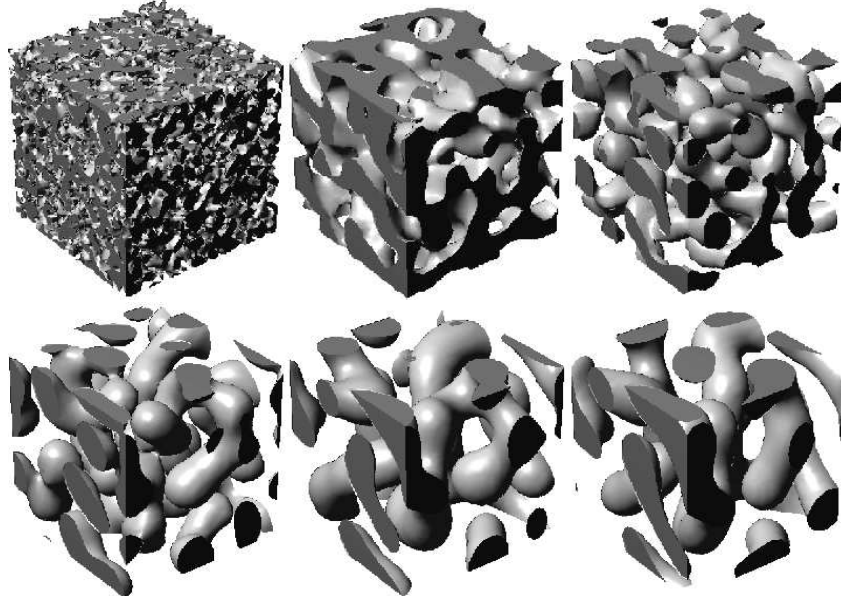


Fig. 7. Phase separation of an asymmetric diblock melt ($f_A = 0.3, f_B = 0.7, N\chi = 20$) in three dimensions. Snapshots were taken at $t = 0, 1, 5, 10, 20$, and 190.

extension beyond the capabilities of previous DSCFT techniques in that it is rigorously tracks the hydrodynamic transport of materials and can be used to study block copolymer dynamics in channels with arbitrarily complex geometries. We presented a pseudo-spectral solution for this model which utilizes fast, parallel Fourier transform routines, making it computationally tractable. We examined several challenging test systems and verified that they produced qualitatively correct results in both two and three dimensions. Furthermore, we validated the hydrodynamic portions of the model by performing a convergence study on the benchmark problem of low Reynolds number flow past a fixed obstacle. We also validated the thermodynamic portions of the model by examining the convergence of phase separating diblock copolymer melts. All three systems we found to converge smoothly to a single solution under mesh size refinement.

References

- [1] F. Drolet, G. H. Fredrickson, Combinatorial screening of complex block copolymer assembly with self-consistent field theory, *Phys. Rev. Lett.* 83 (1999) 43174320.
- [2] G. H. Fredrickson, *The Equilibrium Theory of Inhomogeneous Polymers*, Oxford Press, 2006.
- [3] M. W. Matsen, The standard gaussian model for block copolymer melts, *Journal of Physics* 14 (2002) R2147.
- [4] J. G. E. M. Fraaije, B. A. C. van Vlimmeren, N. M. Maurits, M. Postma, O. A. Evers, C. Hoffmann, P. Altevogt, G. Goldbeck-Wood, The dynamic mean-field density functional method and its application to the mesoscopic dynamics of quenched block copolymer melts, *Journal of Chemical Physics*. 106 (1997) 4260 4269.
- [5] E. Reister, M. Muller, K. Binder, Spinodal decomposition in a binary polymer mixture: Dynamic self-consistent-field theory and monte carlo simulations, *Physical Review E* 64 (2001) 41804.
- [6] R. Hasegawa, M. Doi, Dynamical mean field calculation of grafting reaction of end-functionalized polymer, *Macromolecules* 30 (1997) 3086.
- [7] T. Kawakatsu, Effects of changes in the chain conformation on the kinetics of order-disorder transitions in block copolymer melts, *Phys. Rev. E* 56 (1997) 3240.
- [8] C. Yeung, A. Shi, Formation of interfaces in incompatible polymer blends: A dynamical mean field study, *Macromolecules* 32 (1999) 3637.
- [9] D. Gersappe, Modelling micelle formation in confined geometries, *High Performance Polymers* 12 (2000) 573579.

- [10] G. H. Fredrickson, V. Ganesan, F. Drolet, Field-theoretic computer simulation methods for polymers and complex fluids, *Macromolecules* 35 (2002) 1639.
- [11] R. P. Fynman, A. R. Hibbs, *Quantum Mechanics and Path Integrals*, McGrawHill Book Company, New York, 1975.
- [12] M. Doi, A. Onuki, Dynamic coupling between stress and composition in polymer solutions and blends, *J. Phys. II France* 2 (1992) 16311656.
- [13] K. Schneider, Adaptive wavelet simulation of a flow around an impulsively started cylinder using penalisation, *Applied Computational Harmonic Analysis* 12 (2002) 374380.
- [14] H. Tanaka, Viscoelastic model of phase separation, *Phys. Rev. E* 56 (1997) 44514462.
- [15] G. Fredrickson, Dynamics and rheology of inhomogeneous polymeric fluids: A complex langevin approach, *Journal of Chemical Physics* 117 (2002) 6810.
- [16] G. Tzeremes, K. . Rasmussen, T. Lookman, A. Saxena, Efficient computation of the structural phase behavior of block copolymers, *Phys. Rev E* 65 (2002) 041806.
- [17] J. R. Shewchuk, An introduction to the conjugate gradient method without the agonizing pain (1994). URL <http://www-2.cs.cmu.edu/~jrs/jrspapers.html>
- [18] P. Agnot, C.-H. Bruneau, P. Fabrie, A penalization method to take into account obstacles in incompressible viscous flows, *Numerische Mathematik* 81 (1999) 497520. 25